ORIGINAL PAPER

Structure, mechanical and corrosion properties of DC reactive magnetron sputtered aluminum nitride (AlN) hard coatings on mild steel substrates

B. Subramanian · K. Ashok · M. Jayachandran

Abstract Aluminum nitride (AlN) coatings of about 2 μm thick were deposited on mild steel (MS) by means of direct current (DC) reactive magnetron sputtering. AlN coatings were prepared in an Ar + N_2 gas mixture and their crystal structure, microstructure, and topography were analyzed by X-ray diffractometry (XRD), scanning electron microscopy (SEM) and atomic force microscopy (AFM), respectively. XRD revealed that the films are polycrystalline in nature and have a hexagonal wurtzite structure with a predominant peak observed along the (002) plane. SEM and AFM images showed the presence of continuously covered pebble like spherical grains on the surface. These coatings showed lower coefficient of friction and excellent wear resistance compared to the bare MS substrate. The potentiodynamic polarization studies showed lower corrosion current density and higher polarization resistance for the AlN/MS structure than the uncoated MS substrate.

Keywords Physical vapor deposition · Magnetron sputtering · Aluminum Nitride · Hard coatings · Corrosion resistance

1 Introduction

Aluminum nitride (AlN) is one of the III–V compound semiconductors with many applications in technologically important areas and is considered to be a promising future material for wear-resistant hard coatings due to its high hardness and good mechanical properties [1]. For optoelectronic applications, the hexagonal phase of AlN is used, because of its wide band gap (6.2 eV) [2], high value of surface acoustic velocity [3] and large piezoelectric constant [4]. It acts as an intermediate buffer layer for optical [5] and electronic devices [6] to improve the quality of the epilayer and also as a promising material for optical applications [7], field effect transistors [8]; it has a high resistance to temperature in hostile and corrosive environments [9]. It has been widely used as a dielectric and protective coating [10, 11] and also as a tribological wear and corrosion resistant coating on aluminum and its alloys and on heating elements [12].

These AlN coatings are deposited by many techniques such as molecular beam epitaxy (MBE) [13], ion-beam assisted deposition [14], DC/RF sputtering [15, 16], chemical vapor deposition (CVD) [17], and pulsed laser ablation (PLA) [18]. However, high growth temperature is required for CVD while it is difficult for PLD to develop large area films. In this regard, under specific circumstances where low temperature deposited layers and conformal coatings at relatively low cost are needed, sputtering is the best choice [19].

The performance of an AlN coating is greatly influenced by its microstructure, which is strongly affected by the deposition conditions. Films with various preferred orientations may show different piezoelectric behavior out of which the (002) preferred orientation has been shown to be better [20]. The heat dissipation capacity of AlN films is governed by their microstructure factors such as morphology, interface roughness and preferred orientation. These parameters individually dominate the phonon scattering mechanism/process in AlN films in certain temperature ranges and influence their heat transport properties [21].

B. Subramanian (✉) · K. Ashok · M. Jayachandran
ECMS Division, Central Electrochemical Research Institute,
Karaikudi 630 003, India
e-mail: tspsenthil@yahoo.com

M. Jayachandran
e-mail: Jayam54@yahoo.com

The evolution and variation of preferred orientation with Ar/N_2 (25%/75%) pressure can be explained by the dependence of energy and mobility of the ad atoms and also on the anisotropic growth rate of different lattice planes during the deposition process [22]. Wang et al. [23] characterized AlN films using XPS, which showed the formation of a thin AlON layer at the coating surface due to the absorption of oxygen upon exposure to ambient conditions, whereas the observed Al and N peak positions are consistent with the presence of AlN bonding states within the coating. In this paper, we report the preparation of (002) oriented AlN coatings by the DC reactive magnetron sputtering technique and the material properties characterized by various measurements are presented.

2 Experimental

Layers of AlN were deposited on ultrasonically well-cleaned mild steel substrates using a DC magnetron sputter deposition unit HIND HIVAC. The base vacuum of the chamber was below 1×10^{-6} Torr at a substrate temperature 200 °C. High purity argon was fed into the vacuum chamber for the plasma generation. The substrates were etched for 5 min at a dc power of 50 W and an argon pressure of 10 m Torr (1.33 Pa). The deposition parameters for AlN sputtering are summarized in Table 1 and the film thickness was kept constant about 2 μm for all the studies.

The crystal structure and preferred orientation of the AlN coatings were examined by XRD using PANalytical—3040 X'pert pro diffractometer operated at 40 kV and 30 mA with Cu K_α (1.5414 Å) radiation. The value of texture coefficient, (T_C), was calculated using the equation:

$$T_C = \frac{I_m(hkl)/I_o(hkl)}{\frac{1}{n}\sum_1^n I_m(hkl)/I_o(hkl)} \tag{1}$$

Table 1 Deposition parameters of AlN thin film

Objects	Specification
Target	Al (99.9 %)
Substrate	Mild steel
Target to substrate distance	60 mm
Ultimate vacuum	1×10^{-6} m bar
Operating vacuum	2×10^{-3} m bar
Sputtering gas (Ar:N$_2$)	60:40
Power	180 W
Substrate temperature	200 °C

where I_m (hkl) is the reflected intensity from hkl crystallographic planes in the textured specimen, and $I_o(hkl)$ is the standard intensity, and n is the total number of reflections measured. The T_C value for a particular set of planes (hkl) is proportional to the number of grains that are oriented with this plane parallel to the surface of the specimen. The surface of the coatings was characterized by scanning electron microscopy (SEM) using a Hitachi S 3000H microscope equipped with energy—dispersive X-ray (EDX) spectrometer and a molecular imaging Atomic Force Microscope. The Micro hardness of the films on MS substrates was evaluated using a DM-400 micro hardness tester from LECO with Vickers indenters. A dwelling time of 15 s and a load of 25 and 5 g were used for the measurement.

The Porosity of the coatings was measured using the Ferroxyl test. The test solution was prepared by dissolving 10 g of potassium ferri cyanide ($K_3[Fe(CN)_6]$), 60 g of sodium chloride (NaC1), and 30 g of NH_4Cl in 1 L of warm deionized water. The surface of the coatings was cleaned and degreased with acetone. A piece of filter paper was dipped into the solution (the excess solution was allowed to drain off) and then the wet paper was applied to the test area and allowed to remain undisturbed for 10 min. At the end of the test period the filter paper was removed and tested. Wear tests were carried out in a Block-on-Ring system. All tests were carried out at room temperature, ambient humidity and without lubrication. Steel ball bearing was used as a counter body. The ring material having a diameter of 60 mm was made of High Chromium High Carbon Tool Steel with Vickers hardness 850 HV. The load applied on a specimen was 400 g (3.924 N) with a sliding speed of 100 rpm. The wear rate was calculated by measuring the weight change of a specimen before and after the test. A conventional scratch tester (DUCOM TR-101 M4 Scratch Tester) was used to determine the scratch resistance of the coated layers on MS substrate. The radius of the diamond pin was 0.2 mm. The load applied on a specimen was increased from the initial 2 N to the final 100 N with a loading rate of 5 N mm^{-1} and a loading velocity of 0.2 mm s^{-1}.

Electrochemical polarization studies were carried out using BAS IM6 Electrochemical analyzer. Experiments were conducted using the standard three-electrode configuration, with a platinum foil as the counter electrode, saturated calomel electrode as the reference electrode and the sample as the working electrode. Samples of 1.0 cm^2 exposed area were immersed in the test solution of 3.5% NaCl. Experiments were carried out at room temperature (28 °C). In order to establish the open circuit potential (OCP), prior to the polarization measurements, the samples were immersed in the solution for about 60 min. Impedance measurements were conducted using a frequency response

analyzer and the spectrum was recorded in the frequency range 10 mHz–100 kHz. The applied alternating potential had root mean square amplitude of 10 mV on the OCP. After getting the stable OCP, the upper and lower potential limits of linear sweep voltametry were set at +200 and −200 mV respectively with reference to OCP. The sweep rate was 1 mV s^{-1}. The Tafel plots were also obtained before and after the electrochemical measurements.

3 Results and discussion

3.1 Structural analyses

X-ray diffraction analysis was carried out to investigate the structural properties of AlN coatings on MS substrates deposited at a temperature of 200 °C for 30 min and is shown in Fig. 1. The peak positions are compared with the JCPDS file [No. 025-1133] and the corresponding Miller indices were indexed. Major diffraction peaks of AlN thin films are observed along the (100), (002), (101), and (103) planes. From the XRD analysis it has been observed that the films are single phase possessing hexagonal structure without any other unwanted phases. It exists in the wurtzite phase based on the hexagonal close packing of anions, with one-half of

Fig. 1 XRD spectrum of AlN on mild steel

the tetrahedral sites occupied by the cations [24]. In Bragg–Brentano configuration, by using the broadening of the X-ray peak presented by the scherrer's formula $\beta = 0.9\lambda/D \cos\theta$, where β is the full width at half maximum (FWHM), $\lambda = 1.5414$ Å is the wavelength of the incident X-ray radiation, D is the crystalline diameter, θ is the diffraction angle for the AlN (002) reflection, the crystallite size was calculated to be about 26 nm. The lattice constants values obtained from the XRD data were $a = 0.303$ nm and $c = 0.494$ nm, which are in good agreement with the reported values [25]. The microstructural parameters such as crystallite size, dislocation density, micro strain [26], lattice constant and texture coefficient values were calculated from the XRD pattern and presented in Table 2. For the application of AlN coating in developing surface acoustic wave (SAW) devices, the coatings should have (002) preferred orientation, stoichiometric composition and low surface roughness. The c-axis oriented AlN coatings exhibits excellent piezoelectricity and its surface acoustic wave velocity is up to 5670 ms^{-1}, and the mechanical-electro coupling coefficient is also quite high [23].

The texture coefficient can have profound influence on the properties of thin coatings. The texture coefficient was calculated using Eq. 1 and found to be maximum for (002) orientation. The observation of preferred orientation along (002) plane confirms the formation of stoichiometric AlN coating possessing stronger AlN bonds, which is of the required advantageous properties for developing devices. Further result is similar to that reported in the literature [27], in which it has been proved that the AlN films with (002) preferred orientations are selectively suitable for the development of SAW devices.

3.2 Morphology

Surface morphology of AlN coating examined at a magnification of 40× by scanning electron microscope is shown in the Fig. 2. The coating exhibits pebble or cell-like surface appearance with an average grain size of about 180–200 nm. The micrograph indicates that the cells are composed of tiny grains. Pinhole free surface is
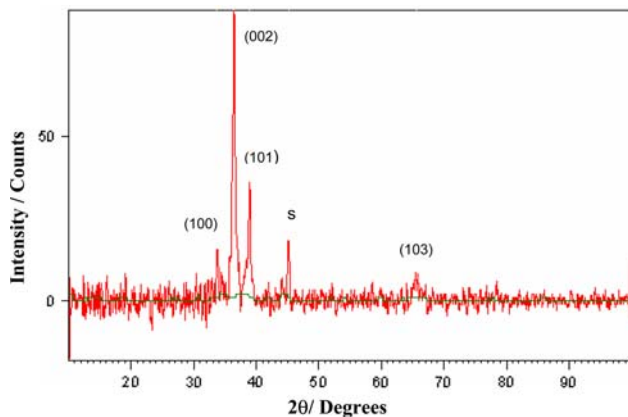
Table 2 Microcrystalline parameters calculated from XRD data

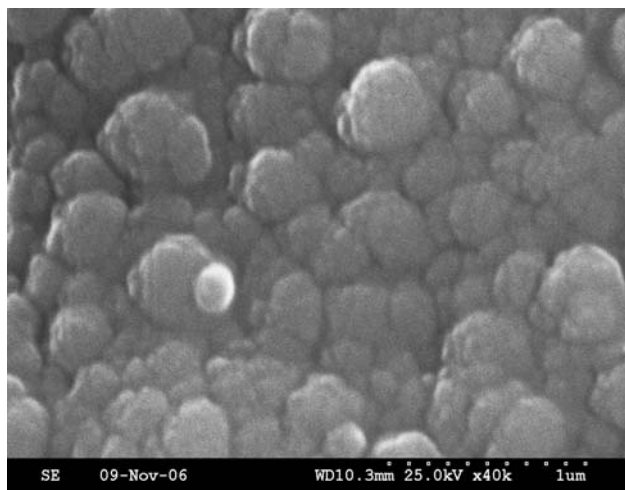| d-Spacing		hkl	Crystallite size (nm)	Dislocation density × 10^{15} (lines m^{-1})	Strain ($\varepsilon \times 10^{-3}$)	Lattice constant (nm)	Texture coefficient (T_C)
Observed (Å)	Standard (Å)						
2.65	2.69	100	28.6	1.22	0.97		0.16
2.46	2.49	002	26.8	1.38	0.97	$a = 0.303$	2.74
2.31	2.37	101	38.1	0.68	0.64	$c = 0.494$	0.83
1.42	1.41	103	16.9	3.48	0.99		0.25

Fig. 2 Surface morphology of AlN coating

observed from SEM and no blue spots were seen on the soaked filter paper after Ferroxyl test. AFM was used to characterize the surface structure and morphology of AlN films. Figure 3 shows uniform surface coverage and the presence of continuous spherical grains on the entire surface as evident from both the 2D and 3D pictures. The average grain size was estimated to be about 170 nm for AlN coatings.

3.3 Hardness, adhesion and wear

The surface hardness values of bare MS and AlN coating on MS were observed with an average of minimum three readings taken at each load. Increase in hardness was observed with the decrease in load. The substrate (anvil) effect is pronounced in case of AlN coatings on MS. The

surface hardness of AlN coatings increased from about 1,300 to about 1,900 HV with the decrease in applied load.

The results of scratch tests, which were done to determine the adhesion strength of the hard coating to the substrate, are shown in Fig. 4. A change in the traction force curve and the coefficient of friction curve is observed at 4.8 mm stroke length, which may be attributed to the mild plastic deformation developed with in the coating during the scratching test. The cohesive failure i.e. failure within the coating occurred at 34 N critical load. An appreciable change in the traction curve at 7.5 mm stroke length and a similar change in the coefficient of friction curve were also observed. In addition, acoustic emission curve also significantly changes with respect to the coefficient of friction, which may be due to the adhesive failure occurred between the coating–substrate interfaces. The coated layer was found to peel off at a critical load of 47.5 N.

The tribological characteristics of the sputtered AlN coatings were measured using block-on-ring test. The ring material used for this test was high chromium high carbon tool steel (850 HV). Low and smooth friction behavior typified by a steady trace at an average value of 0.3 friction coefficient was observed whereas a higher value of 0.5 was observed for the bare substrate. The lower friction coefficient observed in Fig. 5 for the AlN on MS indicated that is stack has better wear resistance. A sufficiently high hardness of the coated layer on any substrate and the superior adhesion of such layer to the substrate are the prerequisite of a hard coating material with excellent wear resistant properties [28]. The AlN coated MS sample showed lower wear rate of 1.0×10^{-5} g mm^{-1} compared to 3.15×10^{-5} mm^3 Nm^{-1} for MS substrate. The wear tracks formed on its surface are shown in Fig. 6. It is explicitly seen that the sample was mainly worn out abrasively and the agglomeration and

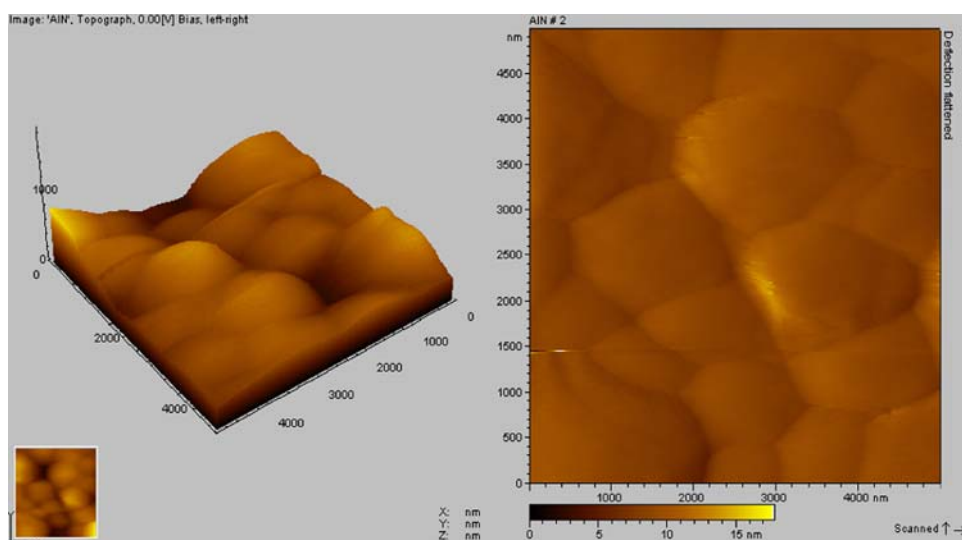**Fig. 3** AFM topography for a scanned area of 5 × 5 μm

Fig. 4 Scratch result for AlN-MS: (a) normal force, (b) traction force, (c) acoustic emission, (d) coefficient of friction
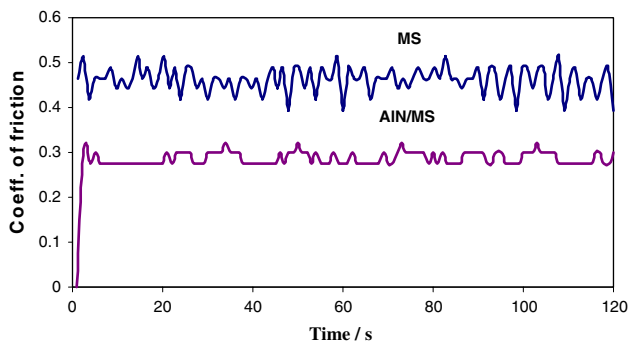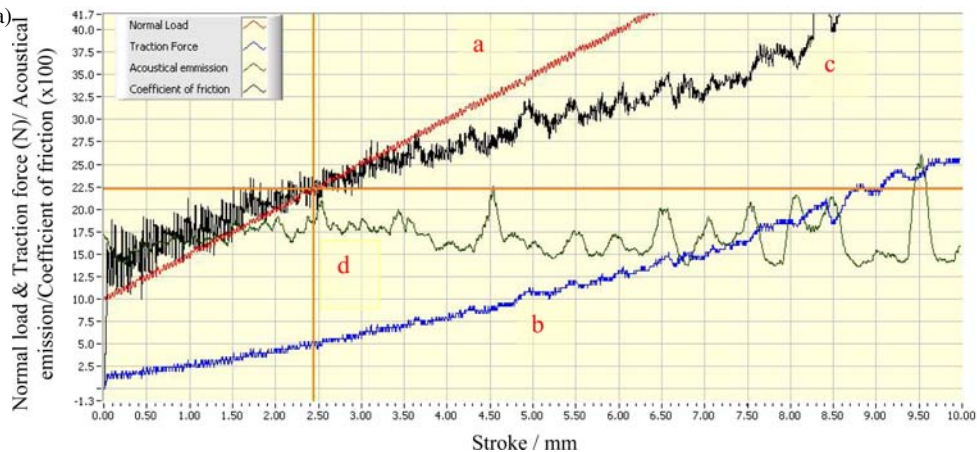

Fig. 5 Variation of friction coefficient with time
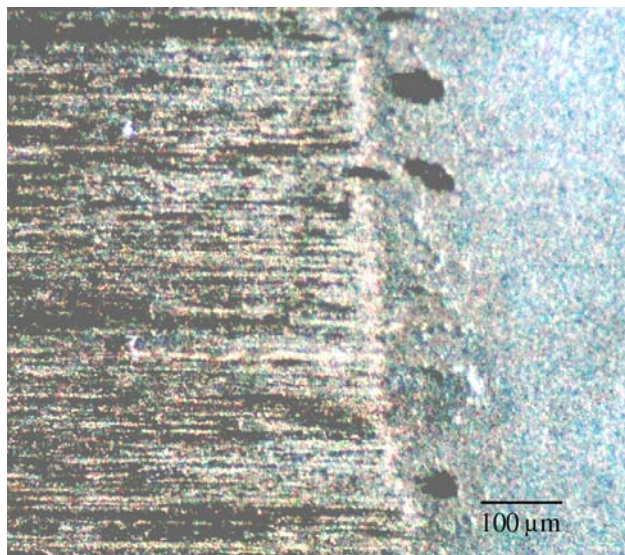

Fig. 6 Optical micrographs of the worn surfaces of AlN coatings

plastic deformation of wear debris are clearly observed in the central region. Jang and Lee [29] have reported that the delamination of the coated layer can be attributed to the inability of the layer to sustain the same amount of elasto-plastic deformation of the softer substrate experienced during the cyclic loading and unloading process.

3.4 Potentiodynamic polarization and AC impedance measurements

To analyze the surface, the material layer was subjected to potentiostatic polarization, one specified potential being impressed on the material at a time. The potentials were either anodic or cathodic with respect to the primary electrochemical process occurring on the surface as indicated by the potentiostatic polarization curves. The potentiodynamic polarization curves obtained for the AlN/MS stack and bare MS substrate in 3.5% w/v NaCl electrolyte are presented in Fig. 7. The E_{corr} and I_{corr} values have been calculated using the Tafel extrapolation method and are given in Table 3. The coated sample shows a positive shift in corrosion potential. The corrosion current is observed to be minimum, 1.5×10^{-4} A cm^{-2}, for the AlN/MS stack as evident from Table 3. There is an appreciable increase in corrosion resistance for the AlN coated MS substrate compared to bare MS substrate.

The same three-electrode cell, as used for the potentiodynamic polarization experiments, was employed for the AC impedance investigations. Impedance measurements were made at OCP applying an AC signal of 10 mV in the
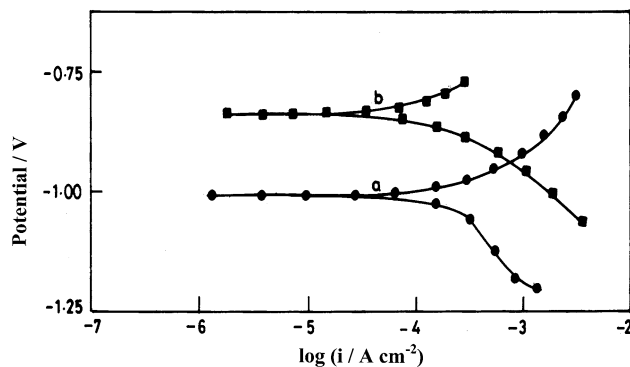

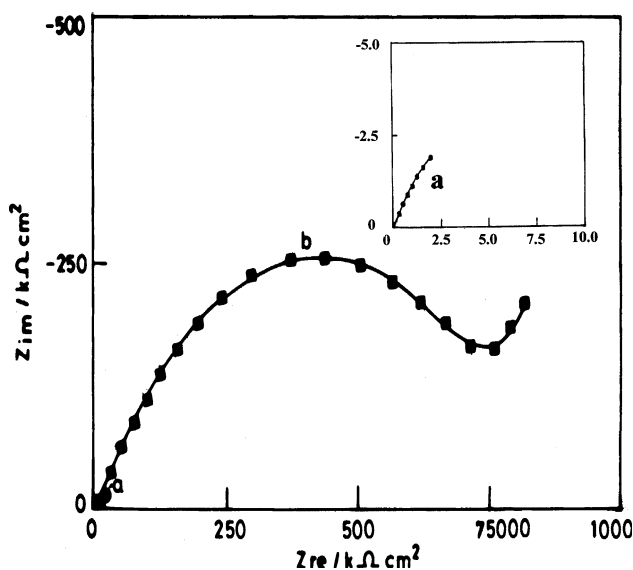**Fig. 7** The potentio dynamic polarization curves in 3.5% NaCl solution for (a) MS substrate, (b) AlN on MS
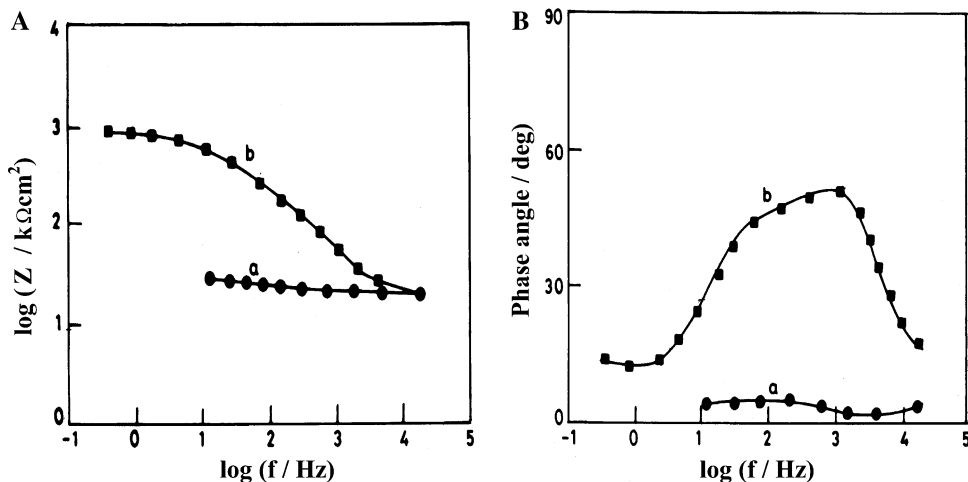
	Sample	E_{corr} vs. SCE (V)	b_a (V dec^{-1})	b_c (V dec^{-1})	I_{corr} (A cm^{-2})	R_{ct} (Ω cm^2)	C_{dl} (F cm^{-2})
Table 3 Polarization and impedance data for bare MS, AlN/MS	MS	−0.99	0.16	−0.31	3.2×10^{-3}	8.6	1.47×10^{-3}
	AlN/MS	−0.84	0.16	−0.14	1.5×10^{-4}	797.2	1.61×10^{-5}

frequency range of 10 mHz–100 kHz. The Nyquist and Bode plots for the samples used for corrosion tests in 3.5% w/v NaCl solution are shown in Figs. 8 and 9, respectively. The double layer capacitance C_{dl} value is obtained from the frequency at which Z imaginary is maximum [30] as given by the equation,

$$\omega\left(Z_{(im)}\, max\right) = 1/C_{dl}R_{ct}. \tag{2}$$

At higher frequencies the interception of real axis in the Nyquist plot is ascribed to the solution resistance (R_s) and at the lower frequencies, the interception with the real axis is ascribed to the charge transfer resistance (R_{ct}). When the sample is immersed in the electrolyte the defects in the coating provide the direct diffusion path for the corrosive media. In this process, localized galvanic corrosion cells are formed and the associated localized corrosion rate is the major contribution in the overall corrosion process. The proposed equivalent circuit for such a system is shown in Fig. 10. The parameters in the equivalent circuit R_{pore} and C_{coat} are related to the properties of the coating and the electrolyte/coating interface reactions respectively. R_{ct} and C_{dl} are related to the charge-transfer reaction at the electrolyte/substrate interface.

The increase in R_{ct} values and decrease in C_{dl} values as shown in Table. 3 for the AlN on MS system confirm its better corrosion resistance property compared to the bare MS substrate. A well-developed semicircular region (Fig. 8) in the case of the AlN on MS stack indicates that this system has maximum corrosion resistance, as observed from the high frequency region of the impedance spectra. The single semicircle behavior obtained may be due to the short exposure time (60 min), which is not sufficient to reveal the degradation of the substrate [31]. Fig 9A (log |z| vs. log f) indicates that the absolute impedance measurements are in the same order. The Bode plot (log f vs. phase angle), Fig. 9B shows a fairly single and narrow peak, indicating one time-constant for the MS substrate whereas a broad peak, observed for the AlN coating on MS substrate, indicates the presence of two interfaces due to the formation of pitting corrosion in the AlN/MS system corresponding to the AlN/electrolyte and MS/electrolyte interfaces.
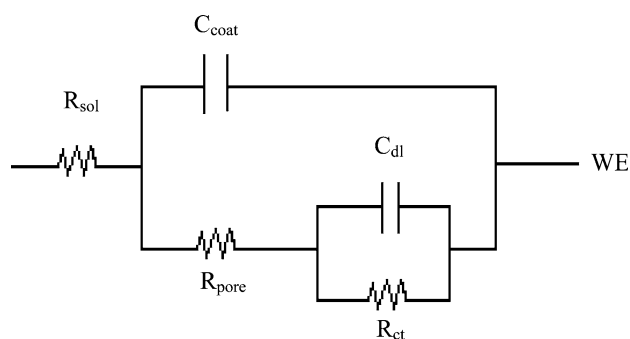

Fig. 8 Nyquist plots of (a) MS substrate, (b) AlN on MS

Fig. 9 (**A**) Bode plots (log |z| vs. log f) of (a) MS substrate, (b) AlN on MS. (**B**) Bode plots (phase angle vs. log f) of (a) MS substrate, (b) AlN on MS

Fig. 10 Equivalent circuit used for fitting the electrochemical impedance data

4 Conclusions

AlN coatings were successfully prepared by reactive DC magnetron sputtering in the gaseous mixture of Ar (60%) and N_2 (40%). XRD results show some degree of polycrystallinity; however, textures could be discerned and pattern indicates that these films have Wurtzite structure with (002) preferred orientation. SEM and AFM observations of the coating show a smooth surface with continuous coverage of pebble like spherical particles. The surface micro hardness of the AlN/MS system has been found to increase with decrease in load. The lower friction coefficient value observed for the AlN on MS indicates that this stack had better wear resistance than the bare MS substrate. The potentiodynamic polarization and the EIS measurements showed that the AlN coating on MS exhibited superior corrosion resistance as compared to the bare MS substrate. The DC magnetron sputtered AlN coating showed significant improvement in the corrosion resistance in 3.5% NaCl solution. A higher positive corrosion potential and a lower corrosion current density were achieved for the AlN coated MS samples.

References

1. Goh YW, Lu YF, Ren ZM, Chong TC (2003) Appl Phys A 77:433
2. Ishihara M, Li SJ, Yumoto H, Akashi K, Ide Y, (1998) Thin Solid Films 316:152
3. Xu XH, Wu HS, Zhang CJ, Jin ZH (2001) Thin Solid Films 388:62
4. Ji XH, Lau SP, Yu GQ, Zhong WH, Tay BK (2004) J Phys D Appl Phys 37:1472
5. Jeon HC, Lee HS, Si SM, Jeong YS, Na JS, Park YS (2003) Curr App Phys 3(4):85
6. Men C, Xu Z, An Z, Chu PK, Wan O, Xie X, Lin C (2002) Appl Surf Sci 199:287
7. Davis RF (1991) Proc IEEE 79:702
8. Wu YF, Keller BP (1996) Appl Phys Lett 69:1438
9. Sungren JE, Hentzel H (1986) J Vac Sci Technol A4:2259
10. Auger MA, Gago R Fernandez M, Sanchez O, Albella JM (2006) Surf Coat Technol 157(1):26
11. Vacandio F, Massiani Y, Gergaud P, Thomas O (2000) Thin Solid Films 359(2):1
12. Dimitrova V, Manova D, Djulgerova R (2000) Surf Coat Technol 123:12
13. Jagannadham K, Sharma AK, Wei O, Kalyanaraman R, Narayan J (1998) J Vac Sci Technol A 16:2004
14. Chu C, Ong PP, Chen HF, Teo HH (1999) Appl Surf Sci 137:91
15. Muhl S, Zapien JA, Mendez JM, Andrade E (1997) J Phys D Appl Phys 30:2147
16. Carlotti G, Gubbiotti G, Hickernell FS, Liaw HM, Socino G (1997) Thin Solid Films 310:34
17. Dobrynin AV (1999) JAppl Phys 85:1876
18. Lu YF, Ren ZM, Chong TC, Cheong BA, Chow SK, Wang JP (2000) J Appl Phys 87:1540
19. Bathe R, Vispute RD, Habersat D (2001) Thin Solid Films 398:575
20. Naik RS, Reif R, Lutsky JJ, Sodini CG (1999) J Electrochem Soc 146:691
21. Balandin A, Wang KL (1998) J Appl Phys 84:6149
22. Hao Cheng, Yong Sun, Peter Hing (2003) Surf Coat Technol 166:231
23. Wang CC, Chiu MC, Shiao MH, Shieu FS (2004) J Electrochem Soc 151(10):F252
24. Chiang YM, Birnie III DP, Kingery WD (1977) Physical ceramics. Wiley, p 31
25. Medjani F, Sanjines R, Allidi G, Karimi A (2006) Thin Solid Films 515:260
26. Williamson GB, Smallman RC (1956) Philos Mag 1:34
27. Lee HC, Kim GH, Hong SK, Lee KY, Yong YJ, Chun CH, Lee JY (1995) Thin Solid Films 261:148
28. Ko KH, Ahn JH, Bae CS, Chung HS (1995) Korean J Mater Res 5:960
29. Jang TS, Lee SW (1998) Mater Chem Phy 54:305
30. Subramanian B, Mohan S, Sobha Jayakrishnan, Jayachandran M (2007) Curr Appl Phys 7:305
31. Liu C, Bi Q, Mathews A (2001) Corr Sci 43:1953